JOM, Vol. 71, No. 4, 2019
https://doi.org/10.1007/s11837-019-03356-4
© 2019 The Minerals, Metals & Materials Society

Multi-material Additive Manufacturing by 3D Plasma Metal Deposition for Graded Structures of Super Duplex Alloy 1.4410 and the Austenitic Corrosion Resistant Alloy 1.4404

KEVIN HOEFER,[1,2] ALEXANDER NITSCHE,[1]
KEVIN GORDON ABSTOSS,[1] GOEKAN ERTUGRUL,[1]
ANDRE HAELSIG,[1] and PETER MAYR[1]

1.—Chair of Welding Engineering, Chemnitz University of Technology, 09126 Chemnitz, Germany. 2.—e-mail: kevin.hoefer@mb.tu-chemnitz.de

In this work, 3D plasma-metal deposition (3DPMD) is introduced as an innovative additive manufacturing process for multi-material components. The possibility of the production of multi-material parts in a layer-by-layer design with 3DPMD was investigated. Multi-material demonstrators with a continuous transition from the super duplex steel 1.4410 to the austenitic steel 1.4404 have been prepared and investigated. By analyzing the hardness, ferrite content, mechanical-technological properties and microstructure, it was shown that the production of multi-material components using 3DPMD is possible. The properties of the transition zone lie between those of the two pure metals. The evaluation of stress–strain curves showed that the strength of the transition zone is higher than that of the austenitic material. It can be concluded that the production of graded steel structures between 1.4404 and 1.4410 using 3DPMD is possible, and mixing of the materials in the transition zone does not weaken the component. The 3DPMD process is suitable to produce functionally graded multi-material components out of metal powders.

INTRODUCTION

Multi-material additive manufacturing (MMAM) enables the rapid and economic production of components with targeted adaption of local properties to real loading conditions. An example is the manufacturing of implants with locally varying porosity and strength, analogous to the natural bone structure.[1–3] A continuous transition between different materials improves the joint strength,[4] reduces mechanical and thermal stresses[5–9] and decreases the crack propagation potential.[10]

Laser-based free-form processes (direct metal deposition, laser-engineered net shaping, laser metal deposition, etc.) currently dominate the field of metallic MMAM.[1,11] Parallel to this, investigations on the manufacturing of functionally graded parts with the friction stir process[12] and the micro-plasma transferred arc (PTA) process are carried out.[13] For the micro-plasma powder process, the higher demands on the powder quality and lower melting rates compared with the classical PTA have been identified as serious disadvantages.

In this work, the freeform, powder- and arc-based additive manufacturing process, designated as 3D plasma metal deposition (3DPMD), was used to produce continuously graded metal parts. 3DPMD is a further development of classic plasma transferred arc welding. Low demands on the powder characteristics (particle size, surface structure), high deposition rates (up to 10 kg/h) and the possibility of mixing up to four different powders simultaneously during the process are the greatest advantages of this process.

Detailed information on the process, the materials that can be processed and application examples have been published elsewhere.[14–16]

The majority of the actual state-of-the-art research is focusing on the additive manufacturing of mono-material components, for example, in super

(Published online February 7, 2019)

duplex alloys.[17] or austenitic corrosion resistant steels.[18–20] This article elaborates on the production of metallic multi-material components. The continuous transition from a ferromagnetic super duplex alloy (1.4410) to a non-magnetic austenitic alloy (1.4404) is realized as a demonstration part. Due to the variable ferrite contents as a function of the part height, this material combination is highly suitable as an indicator material to study the transition from one steel to another. This allows a reliable evaluation of the multi–material structure and its properties.

MATERIALS AND METHODS

Raw Materials

The super duplex steel 1.4410 and the austenitic corrosion-resistant steel 1.4404 were used in this study in powder form. Both powders are characterized by a spherical particle shape and a particle size between 50–l50 μm (Fig. 1). The chemical compositions of the powder materials are shown in Table I. It should be noted that the content of nickel in 1.4410 is higher than the specification limit described in the standard,[21] but this is not critical for this work.

Multi-material Additive Manufacturing

A stainless steel plate (alloy 1.4301) with a thickness of t = 12 mm was used as building platform. As a demonstrator geometry, walls with a height of h = 48 mm and a wall thickness of t = 7 mm were manufactured in 45 passes in total. The transition from the super duplex alloy to the austenitic structure starts from the 13th layer onwards. The transition area consists of 14 layers and is defined by a set volume ratio of 1:1 of the two powders. From layer 28 onwards, the structure is finished in 17 layers using 100% austenitic steel powder.

The parameters of the build cycle are defined by a layer thickness of z = 1.5 mm, a welding current of I = 140 A, an interpass temperature of t = 100°C and a welding speed of v = 8 mm/s. High-purity argon was used as shielding gas with 12 l/min and as plasma gas with 1.5 l/min.

Characterization

First, the powder shape was characterized by means of a scanning electron microscope (SEM) using a Tescan Mira 3. The assessment of the microstructure and mechanical-technological properties was carried out in the "as-welded" condition.

The microstructure was analyzed using a Zeiss optical microscope and an FEI Nova NanoSEM 450 scanning electron microscope. Standard metallographic procedures were used to prepare specimens. The etching for macrographs was carried out in a 15% aqueous HCl solution for 30 min. Additional specimens were prepared with the Beraha type 2 color etchant (15 s) to distinguish different phases.

The ferrite content was determined with a magnetic inductive measurement system, Fischer FERRITSCOPE MP3, over the entire cross-section.

For investigation of the mechanical properties, in total 20 micro-tensile specimens were produced by eroding and grinding. A forming and quenching dilatometer type DIL 805 A/D from Bähr was used to carry out the tensile tests. In addition, mapping of the micro-hardness of every layer was carried out with a Durascan 70 automated hardness indenter.

RESULTS AND DISCUSSION

Microstructure

Figure 2a provides an overview of the cross-section of the multi-material part. In general, Fig. 2a shows no inter-run fusion defects or porosity within the structure. The characteristic dual-phase structure of austenite and ferrite of the super duplex alloy 1.4410 is shown in Fig. 2b and e. It can be seen that the ferrite phase (dark area) is present as a dendritic structure in an austenitic matrix (light area). Color etching with the Behara type 2 clearly identified the dark areas as δ-ferrite. Sigma phase formation with slow cooling of the

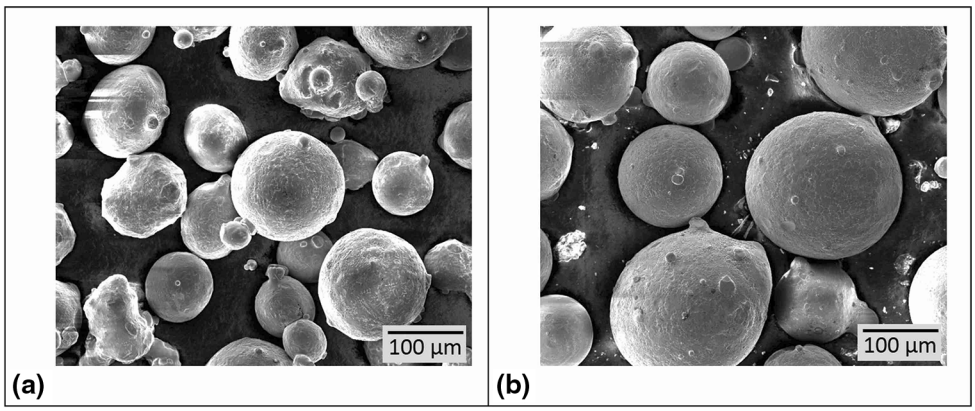

Fig. 1. Characteristic shape of the raw material powders. (a) SEM image of 1.4404 powder; (b) SEM image of 1.4410 powder.

Table I. Chemical composition of powders according to manufacturer specifications in wt.%

Grade	C	Ni	Cr	Mn	Si	Mo	N	Cu	Fe
1.4410	0.02	9.8	25.1	0.60	0.40	4.20	0.3	0.01	Base
1.4404	< 0.03	13.0	17.0	1.0	1.0	2.0	–	–	Base

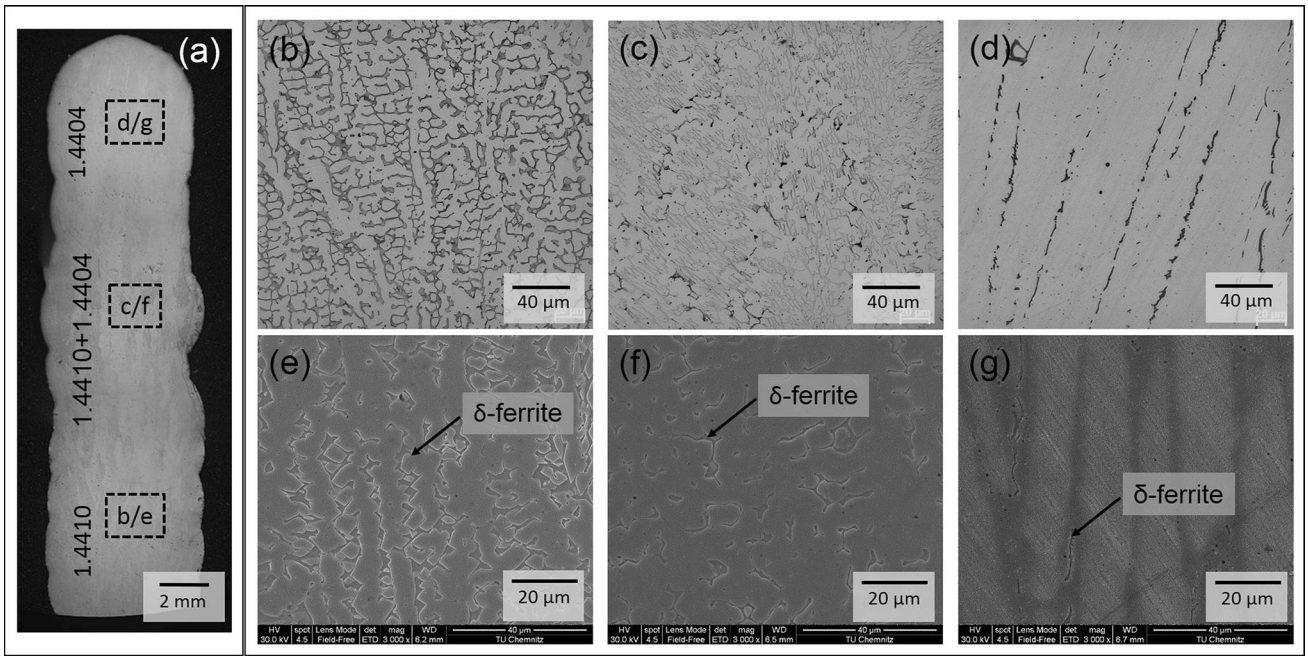

Fig. 2. Macrograph and micrographs of the weld metal at different locations: (a) macro cross section of the multi-material part with sampling locations; (b) optical micrograph of 1.4410; (c) optical micrograph of hybrid structure with 50% 1.4410 and 50% 1.4404; (d) optical micrograph of 1.4404; (e) SEM image of 1.4410; (f) SEM image of the hybrid structure with 50% 1.4410 and 50% 1.4404; (g) SEM image of 1.4404.

material was not confirmed. Sigma phase would appear as white zones because of the lack of response of the color etchant. The zone of the mixed structure of 1.4410 and 1.4404 is shown in Fig. 2c and f. The dark ferrite phase is present in austenite with a lower fraction as observed in the pure 1.4410 structure. The color etching also revealed that no segregated areas formed. The transition zone is therefore characterized by a homogeneous structure, and the individual areas merge continuously without demixing or accumulation of single elements. The structure of the austenitic corrosion-resistant steel 1.4404 shows an almost completely austenitic matrix with residual ferrite in the form of lines (Fig. 2d). Figure 2g clearly shows that the residual ferrite is mainly located at the grain boundaries of the austenite grains.

Ferrite Content

Figure 3 shows the ferrite content in the multi-materials components as a function of part height. The highest values were measured in the area of 1.4410 with an average of 18%. However, the measured value deviates strongly from the estimated value using the WRC 1992 diagram[22] (Fig. 4). A theoretical ferrite content of 35% was determined in the diagram. The lower ferrite

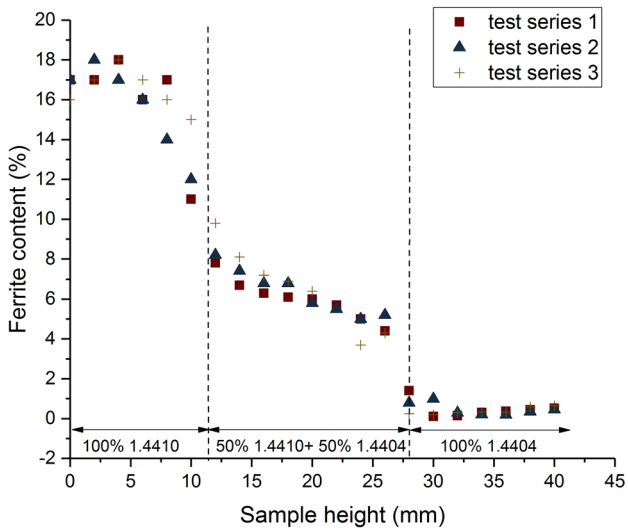

Fig. 3. Measured ferrite content in percent across the entire component height for three parts.

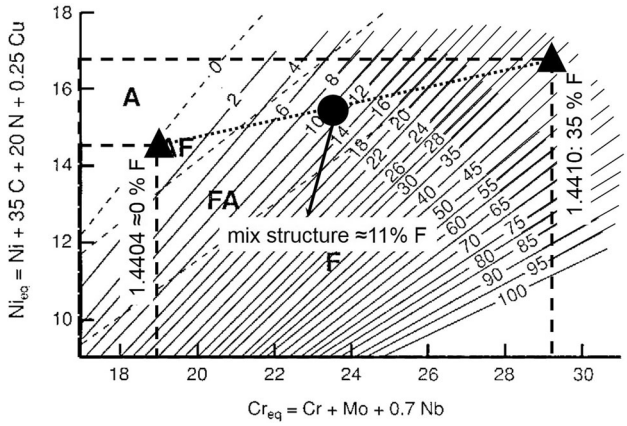

Fig. 4. WRC-92 diagram of the raw materials revealing the transition from duplex to austenitic structure (A = austenite, AF = austenite + ferrite, FA = ferrite + austenite, F = ferrite).

content in the present work has its origin in the process-related repeated reheating of the weld. As a result, the temperature ranges between 1200°C and 800°C, which is critical for super duplex alloys, and is passed several times, resulting in very long cooling times. Previous investigations have shown that the critical cooling time is between 1200°C and 800°C $t_{1200-800}$ = 150 s.[14] These extremely long cooling times promote the formation of austenite and are thus the main reason for the measured low ferrite contents. In the transition area, an average ferrite content of 8.3% was determined. The deviations from the calculated value (11%) are lower compared with the area of the pure super duplex alloy. The location of the multi-material zone in the middle of the component leads to faster cooling conditions because of the transition from two- to three-dimensional heat conduction. In the upper component area, the heat dissipation via the building platform is additionally accompanied by the convection effect with the environment of the part surface. The shorter cooling times associated with this are an explanation for the smaller differences between the theoretical and real ferrite contents in the transition zone. Only very small amounts of residual ferrite were determined in the upper, pure austenitic area of the part. The austenitic microstructure of the 1.4404 was thus maintained and corresponds to the estimated value.

Hardness

The results of the hardness line measurements shown in Fig. 5a complement and confirm the ferrite measurements and metallography described above. A continuous decrease of the hardness values can be observed over the height of the component. With an average of 280 HV1, the pure 1.4410 region shows the highest hardness values in the part. The transition zone with a hardness of approximately 220 HV1 lies between the hardness of the two pure steels. This also indicates a smooth transition and homogeneous mixing between the two alloys. The austenitic material 1.4404 is specified with an average hardness of 163 HV1. Furthermore, it should be noted that no sharp boundaries between materials in terms of hardness values were determined. The reason for this is the dilution of the lower layers during welding. Dilution is defined as the degree of mixing of the lower weld deposit with the subsequent layer. The process-specific degree of dilution of the 3DPMD process is around 23%.[14]

Compared with the results presented in the literature, a slight hardening of plus 40 HV can be determined for the 1.4410 steel.[21] In the upper component area (1.4404), there is a significant reduction in hardness compared with the data presented in the literature. Material 1.4404 is described in the literature with a hardness of 225 HV.[21] Detailed investigations of the austenitic region (Fig. 5b) show minimal hardness peaks. However, no discontinuities could be detected because of the layer-wise structure. Figure 5c shows a hardness mapping of the transition zone from the austenitic alloy to the transition zone. Gradients in the hardness can be recognized. The top part of the mapped area is the austenitic matrix. The transition zone starts from y = -2 mm and is characterized by a higher hardness. In the range between y = -– 1 mm and y = – 2 mm, an average hardness exists because of the process-specific dilution.

Tensile Tests

Figure 6a shows the results of the micro-tensile tests. The graphs show the stress–strain curves of a single specimen of each position. In total, four tensile tests per specimen position were performed. The position of the tensile specimens extracted from the part is sketched in Fig. 6c.

For material 1.4410 (Graph A), strength properties within the technical specifications are observed.[23] The strength of the austenitic alloy is below the specification limit.[23] This is in line with the low hardness values. The loading direction for these samples was perpendicular to the building direction. The strength of the super duplex alloy is in the upper limit range of the technical specification and for the austenite close to the lower specification limit. This also corresponds to the results of the hardness measurements. The ductility shows opposite trends.

For the transition area, tensile tests were carried out in three different load directions (B, C, D). Compared with 1.4404, enhanced values were obtained perpendicular to the build direction (B). It can be assumed that the increased ferrite content in the microstructure leads to the increased strength. In case of loading in build direction (D), the tensile strength is reduced by 14% compared with the orientation perpendicular to the build direction. The evaluation of the fracture patterns showed that the location of the failure is always close to the austenitic side; see Fig. 6b. Subsequent heat

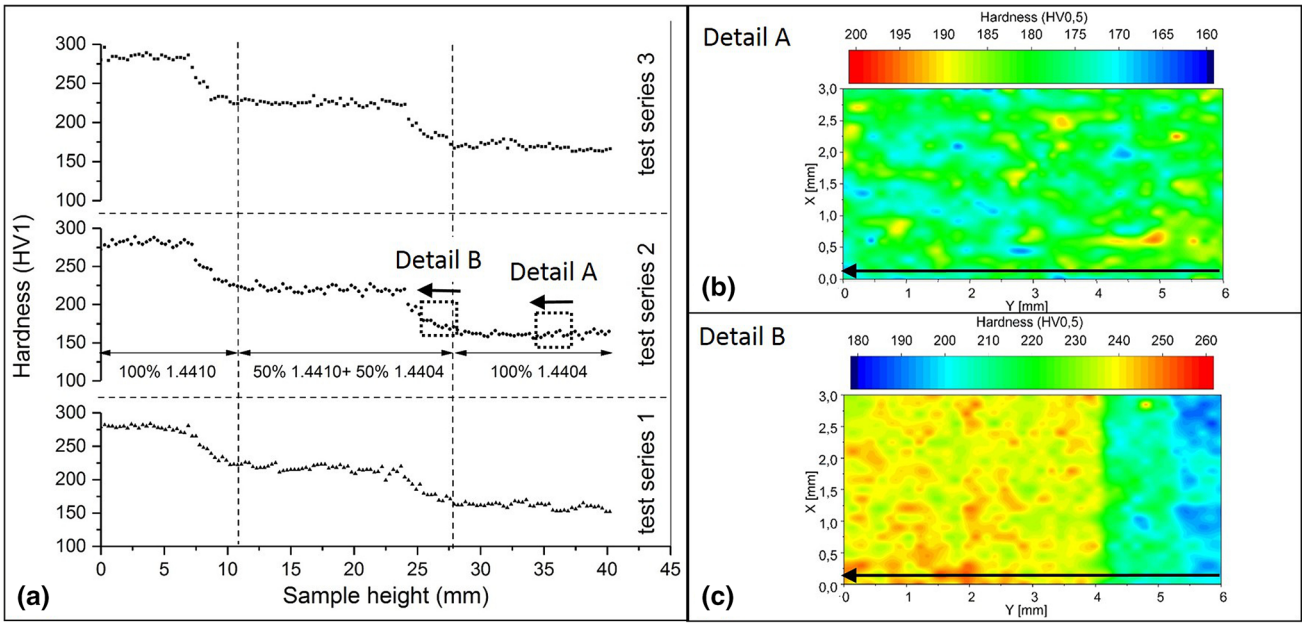

Fig. 5. Results of the hardness measurements: (a) hardness line scans with 140 indents with a distance of 0.5 mm; (b) hardness mapping of 1.4404 with 860 indents with a distance of 0.15 mm; (c) hardness mapping of the changeover from 1.4404 to the transition zone with 860 points with a distance of 0.15 mm.

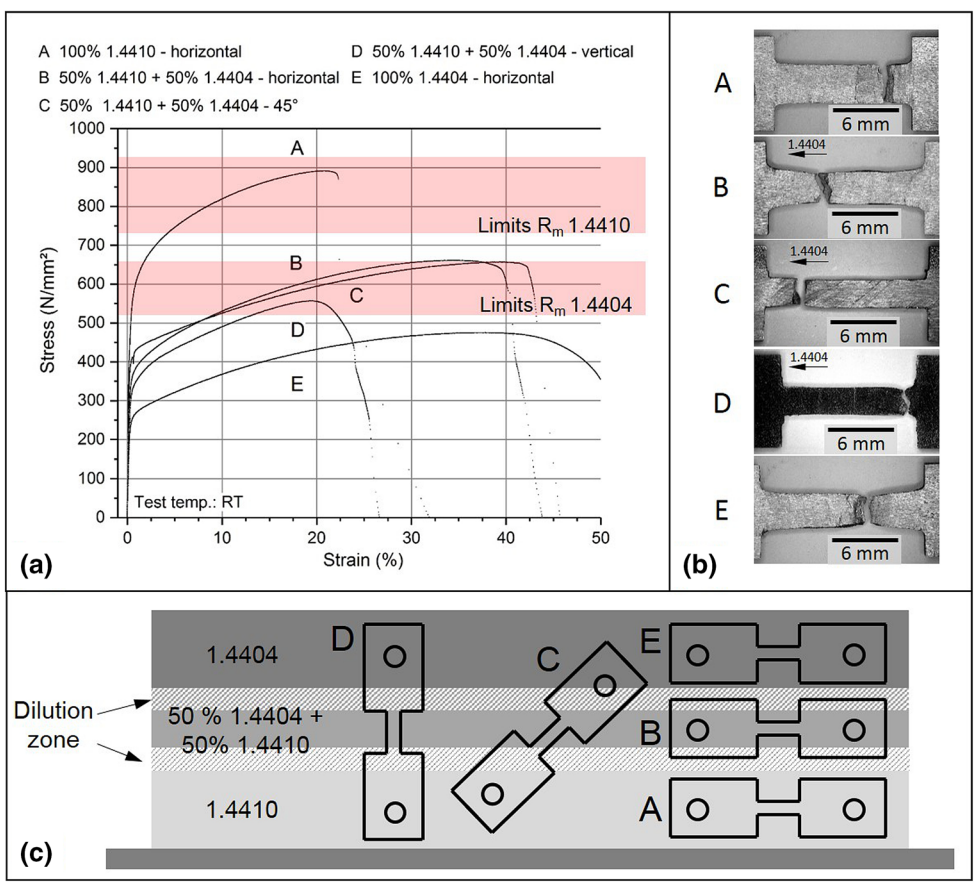

Fig. 6. Overview of the tensile test results: (a) representative stress–strain diagrams; (b) representative fracture patterns; (c) schematic of the tensile specimen position.

Table II. Results of the micro-tensile tests

	Sample labeling	$R_{p0.2}$ (N/mm^2)	R_M (N/mm^2)	$R_{p0.2}/R_M$ (%)	F_{max} (N)	A (%)
A	100% 1.4410	533	875	60.1	5095	23.9
	Horizontal	$\sigma = 0$	$\sigma = 26.2$	$\sigma = 1.8$	$\sigma = 275.8$	$\sigma = 2.9$
B	50% 1.4410 + 50% 1.4404	368	648	56.9	3808	56.9
	Horizontal	$\sigma = 4.2$	$\sigma = 21.9$	$\sigma = 2.5$	$\sigma = 328.5$	$\sigma = 2.5$
C	50% 1.4410 + 50% 1.4404	413	669	61.7	2528	42.7
	45°	$\sigma = 0.7$	$\sigma = 18.4$	$\sigma = 1.6$	$\sigma = 74.2$	$\sigma = 0.9$
D	50% 1.4410 + 50% 1.4404	332	560	59.2	2231	25.4
	vertical	$\sigma = 12.3$	$\sigma = 25.0$	$\sigma = 0.9$	$\sigma = 57.5$	$\sigma = 5.0$
E	100% 1.4404	244	460	52.9	2715	47.4
	Horizontal	$\sigma = 11.3$	$\sigma = 12.6$	$\sigma = 1.2$	$\sigma = 205.7$	$\sigma = 3.7$

σ stands for standard deviation.

treatment could reduce this effect but was not part of this study. Shear loading (45° specimen orientation, C) of the transition zone results in average strength properties, but an increased elongation.

In total, it can be concluded that the strength of the transition zone is higher than that of the pure austenitic material, so that despite the mixed structure, no weakening of the part is observed.

The mean values of the static tensile tests are summarized in Table II.

CONCLUSION

The suitability of the 3DPMD process for the additive manufacturing of multi-material components was studied for the transition from an austenitic steel to a super-duplex steel alloy. The metallurgical evaluation of cross sections showed a homogeneous microstructure with an even transition between the different materials. It was also demonstrated that the process characteristics do not result in sharp boundaries between the materials because of the process-specific dilution. The homogeneous mixing of the two steels was demonstrated by metallography, hardness measurements and the measurement of ferrite content. The micro-tensile tests showed that the direction of loading has a decisive influence on the achievable strength properties. Strength was lowest for the pure austenitic region. For the transition zone, a pronounced anisotropic behavior has been proven. In the transition zone, the highest tensile strengths were observed for the specimens oriented perpendicular to or 45° to the build direction. The evaluation of the fracture patterns showed that the failure of the tensile specimens in the transition region always occurred close to the austenitic area, so that the transition zone itself is not the weak point of the component.

In summary, 3DPMD was qualified as a potent process in multi-material additive manufacturing of transition structures from austenitic to super-duplex steel grades. Defect-free structures with a smooth transition with complete mixing in the transition zone were produced. The process offers great potential for other metal transitions.

REFERENCES

1. A. Bandyopadhyay, B.V. Krishna, W. Xue, and S. Bose, *J. Mater. Sci. Mater. Med.* 20, 29 (2009).
2. J. Parthasarathy*, B. Starly, and S. Raman, *J. Manuf. Process.* 13, 160 (2011).
3. L.E. Murr, S.M. Gaytan, E. Martinez, F. Medina, and R.B. Wicker, *Int. J. Biomater.* 28, 1–14 (2012).
4. S. Sampath, H. Herman, N. Shimoda, and T. Saito, *MRS Bull.* 20, 27 (1995).
5. S. Suresh, A.E. Giannakopoulos, and J. Alcalá, *Acta Mater.* 45, 1307 (1997).
6. A.E. Giannakopoulos and S. Suresh, *Int. J. Solids Struct.* 34, 2393 (1997).
7. A.E. Giannakopoulos, S. Suresh, M. Finot, and M. Olsson, *Acta Metall. Mater.* 43, 1335 (1995).
8. R.L. Williamson, B.H. Rabin, and J.T. Drake, *J. Appl. Phys.* 74, 1310 (1993).
9. J.T. Drake, R.L. Williamson, and B.H. Rabin, *J. Appl. Phys.* 74, 1321 (1993).
10. F. Erdogan, *Compos. Eng.* 5, 753 (1995).
11. I. Yadroitsev, L. Thivillon, Ph. Bertrand, and I. Smurov, *Appl. Surf. Sci.* 254, 980 (2007).
12. R.M. Mirandaa, T.G. Santosa, J. Gandrab, N. Lopesa, and R.J.C. Silva, *J. Mater. Process. Technol.* 213, 1609 (2013).
13. H. Zou, H. Zhang, W. Guilan, and J. Li, in *Electromagnetics Research Symposium* (Moskau), 1953 (2009).
14. K. Höfer, A. Hälsig, and P. Mayr, *Weld World* (2018). https://doi.org/10.1007/s40194-017-0527-9.
15. K. Höfer, C. Teichgräber, P. Mayr, M. Berger, *FüMoTeC* 2, 1 (2017), ISBN 978-3-96100-034-0.
16. K. Höfer, A. Hälsig, P. Mayr, *DVS Bericht*, 337, 297 (2017), ISBN: 978-3-96144-008-5.
17. G. Posch, K. Chladil, and H. Chladil, *Weld World* 61, 873 (2017).
18. S. Cheruvathur, E.A. Lass, and C.E. Campbell, *JOM* 68, 930 (2016).
19. W. Hofmeister and M. Griffith, *JOM* 53, 30 (2001).
20. L. Jiapeng, J. Xiao, G. Ruinan, P. Zhou, Y. Huang, J. Sun, and M. Yan, *Metals* 8, 548 (2018).
21. Stahlschlüssel, Version 8.0, Edition 24 (2016).
22. D.J. Kotecki and T.A. Siewert, *Weld J* 5, 171 (1992).
23. DIN EN 10088-2 (2014).

Publisher's Note Springer Nature remains neutral with regard to jurisdictional claims in published maps and institutional affiliations.